Hindawi
Geofluids
Volume 2021, Article ID 6639793, 11 pages
https://doi.org/10.1155/2021/6639793

Research Article

In Situ Stress Prediction in Subsurface Rocks: An Overview and a New Method

Yushuai Zhang,[1] Shangxian Yin,[2] and Jincai Zhang[3]

[1]*College of Earth Science and Engineering, Shandong University of Science and Technology, Qingdao, Shandong, China*
[2]*North China Institute of Science and Technology, Yanjiao, China*
[3]*Sinopec Tech Houston, Texas, USA*

Correspondence should be addressed to Shangxian Yin; yinshx03@126.com and Jincai Zhang; zhangjincai@yahoo.com

Received 17 January 2021; Revised 5 March 2021; Accepted 27 March 2021; Published 20 April 2021

Academic Editor: Yongcun Feng

Methods for determining in situ stresses are reviewed, and a new approach is proposed for a better prediction of the in situ stresses. For theoretically calculating horizontal stresses, horizontal strains are needed; however, these strains are very difficult to be obtained. Alternative methods are presented in this paper to allow an easier way for determining horizontal stresses. The uniaxial strain method is oversimplified for the minimum horizontal stress determination; however, it is the lower bound minimum horizontal stress. Based on this concept, a modified stress polygon method is proposed to obtain the minimum and maximum horizontal stresses. This new stress polygon is easier to implement and is more accurate to determine in situ stresses by narrowing the area of the conventional stress polygon when drilling-induced tensile fracture and wellbore breakout data are available. Using the generalized Hooke's law and coupling pore pressure and in situ stresses, a new method for estimating the maximum horizontal stress is proposed. Combined it to the stress polygon method, a reliable in situ stress estimation can be obtained. The field measurement method, such as minifrac test, is also analyzed in different stress regimes to determine horizontal stress magnitudes and calibrate the proposed theoretical method. The proposed workflow combined theoretical methods to field measurements provides an integrated approach for horizontal stress estimation.

1. Introduction

In situ stresses are consisted of the vertical stress and the maximum and minimum horizontal stresses. They are very important parameters for subsurface engineering planning and modeling. For example, hydromechanical behaviors of natural and hydraulic fractures are strongly dependent on the in situ stresses. Hydraulic fractures for enhanced oil and gas production are generally created approximately perpendicular to the minimum stress direction and propagate along the other two stress directions [1]. Therefore, fully understanding in situ stresses is crucially important for horizontal well planning and hydraulic fracture design. For instance, in an on-azimuth well (i.e., the horizontal well placed along the direction of the minimum stress) of the Marcellus shale gas play, the productivity increased 40-50% compared to a 45° off-azimuth well [2]. The minimum horizontal stress is also an important parameter for other geomechanical analyses, such as borehole and excavation stability. For instance, Li et al. [3] developed an advanced and useful hydromechanical model that is capable to simulate progressive wellbore breakout during drilling, and the simulation results demonstrated that the magnitude of the minimum horizontal stress to a large extent controls breakout magnitude, while its orientation determines breakout direction.

Microseismic measurements in the Permian basin demonstrate that the minimum horizontal stress controls hydraulic fracture growth and propagation, as shown in Figure 1. This figure demonstrates that hydraulic fracturing in stage 2 in a vertical well was performed at the interface of two formations with high and low minimum horizontal stresses, respectively. It can be seen from Figure 1 that the hydraulic fractures interpreted from microseismic measurements mainly developed in the rock having a lower minimum horizontal stress and only partially grew in the rock having a higher minimum horizontal stress. Furthermore,

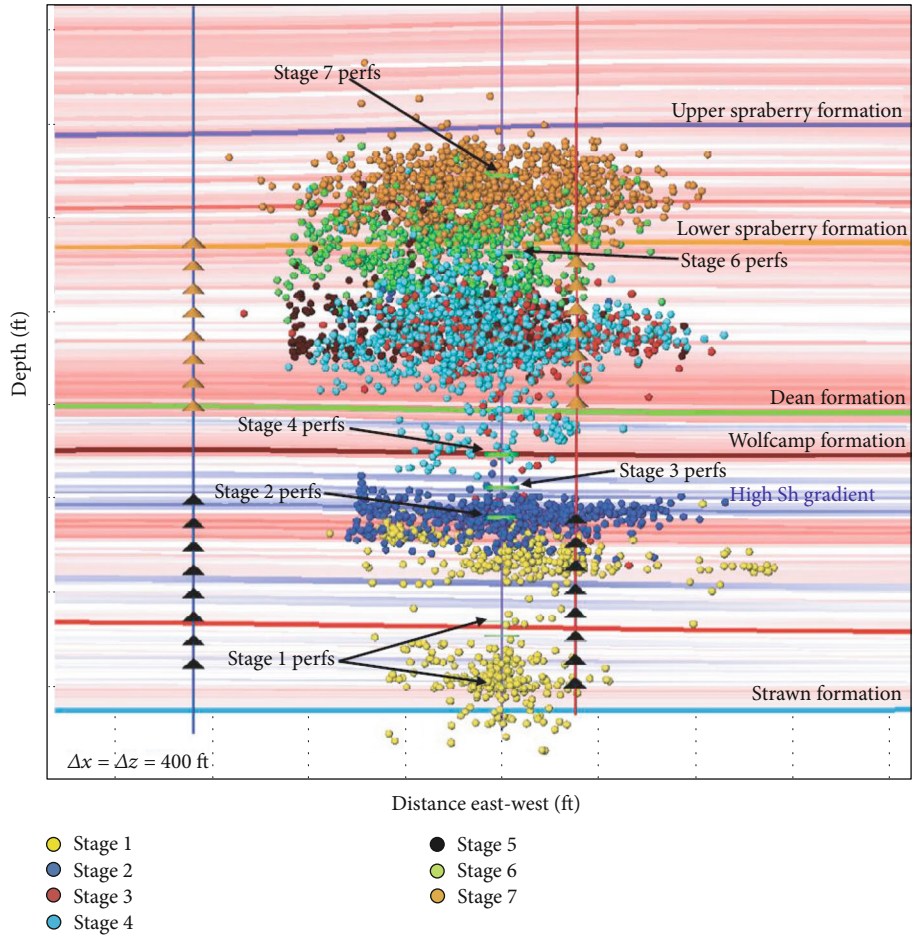

Figure 1: A longitudinal view showing the length and height of the microseismic interpreted hydraulic fractures in different stages. A cross-section of the minimum horizontal stress gradient is also presented in this figure. The dots are observed microseismic events color coded by different stages. The red, white, and blue colors in the background indicate low, middle, and high minimum stress (Sh) gradients, respectively [9].

the hydraulic fractures could not penetrate through the formation having a high minimum horizontal stress. In other words, the fractures were unable to propagate further up because of this high stress, as shown in stage 2 of Figure 1. It indicates that the high minimum horizontal stress formation is a barrier for the propagation of hydraulic fractures. In contrast, the hydraulic fractures grew far beyond the perforation formation where the minimum horizontal stress was small (such as stages 3-7). The same conclusion was obtained in other field observations [4].

In situ hydraulic fracturing mined-back observations also demonstrate that the minimum horizontal stress variation is a major factor to dominate the growth and curvature of hydraulic fractures. The hydraulic fractures stop propagation in the rock that has a high minimum horizontal stress, as shown in Figure 2. It indicates that a rock having a high minimum horizontal stress acts as a containment for terminating hydraulic fracture growth. Therefore, accurately determining horizontal stresses is a precondition for optimizing horizontal well drilling and completion and for providing a better design for hydraulic fracturing.

The most difficult task in in situ stress analyses is to determine the minimum and maximum stresses, because the vertical or overburden stress can be directly calculated from the density logs [5]. The minimum and maximum horizontal stresses in the oil and gas industry are commonly estimated from borehole injection tests. However, these data are generally unavailable in a new project (e.g., [6, 7]). Numerical modeling, such as the finite different and finite element methods (e.g., [8]), can be applied to model in situ stresses; however, the boundary conditions and tectonic stresses are needed for the modeling, which are not easy to be obtained. Therefore, challenges are still presence in measuring and theoretically estimating the horizontal stresses. In this paper, we introduce some commonly used approaches to estimate in situ stresses, primarily the maximum and minimum horizontal stresses, then provide an integrated method to calculate the horizontal stresses.

2. Determination of Horizontal Stresses from Theoretical Derivations

2.1. Theoretical Derivation of Horizontal Stresses from Linear Elasticity. During the sedimentary process in the geologic time, the rocks might have experienced both elastic and plastic deformations. However, in the contemporary stress state,

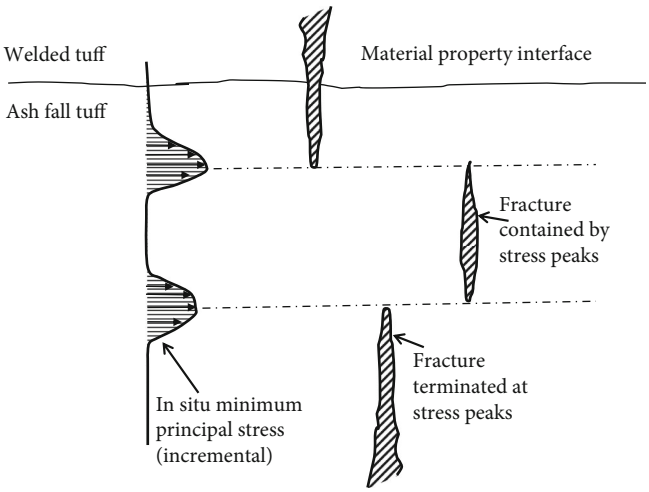

Figure 2: The minimum horizontal stress profile and hydraulic fracture growth and termination plotted based on hydraulic fracture mined-back measurements ([10] with modification).

the formation deformations can be approximately described using the theory of elasticity. The minimum and maximum horizontal stresses can be derived from the generalized Hooke's law with coupling pore pressure and in situ stresses from linear elasticity. For a vertical transversely isotropic rock, the minimum and maximum horizontal stresses can be calculated in the following equations [11]:

$$\sigma_h = \frac{E_h \nu_V}{E_V(1-\nu_h)}\left(\sigma_V - \alpha_V p_p\right) + \alpha_h p_p + \frac{E_h}{1-\nu_h^2}\varepsilon_h + \frac{E_h \nu_h}{1-\nu_h^2}\varepsilon_H + \frac{E_h \alpha_{Th}}{1-\nu_h}\Delta T, \quad (1)$$

$$\sigma_H = \frac{E_h \nu_V}{E_V(1-\nu_h)}\left(\sigma_V - \alpha_V p_p\right) + \alpha_h p_p + \frac{E_h}{1-\nu_h^2}\varepsilon_H + \frac{E_h \nu_h}{1-\nu_h^2}\varepsilon_h + \frac{E_h \alpha_{Th}}{1-\nu_h}\Delta T, \quad (2)$$

where σ_V is the vertical stress which can be calculated by integrating the bulk density logs; σ_h and σ_H are the minimum and maximum horizontal stresses, respectively; E_V and E_h are Young's moduli in vertical and horizontal directions (refer to Figure 3), respectively; ν_V and ν_h are Poisson's ratios in vertical and horizontal directions, respectively; α_V and α_h are Biot's coefficients in vertical and horizontal directions, respectively; ε_h and ε_H are the strains in the minimum and maximum horizontal stress directions, respectively; α_{Th} is the thermal expansion coefficient in the horizontal direction; ΔT is the increase in temperature of the formation. For the case of a borehole, $\Delta T = T_w - T_f$ and T_f and T_w are the rock and borehole mud temperatures, respectively.

Most shale formations, due to their abundant bedding planes, belong to rocks of vertical transverse isotropy (VTI), and the horizontal stresses can be obtained using Eqs. (1) and (2). Poisson's ratios and Young's moduli of a shale are very different in the vertical and horizontal directions. This causes the horizontal stresses in the shale to be very different

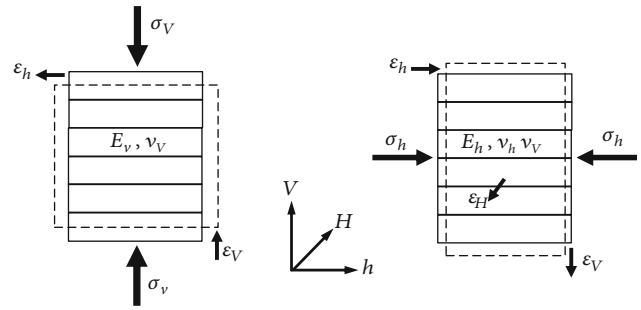

Figure 3: A vertical transversely isotropic rock showing Poisson's ratios and Young's moduli in two different loading directions.

to the ones in the isotropic rock (such as sandstone). Generally, a shale has a much higher horizontal Young's modulus than the vertical one (e.g., $E_h = 1.438E_V$ from experimental tests in shales in [11]); therefore, from Eqs. (1) and (2), the VTI rock may have a higher horizontal stress than the isotropic rock. Thiercelin and Plumb (1994) gave similar solutions to Eqs. (1) and (2) without consideration of the thermal effect. In an isotropic case, Eqs. (1) and (2) can be simplified to the following forms because $E_h = E_V = E$, $\nu_h = \nu_V = \nu$, $\alpha_h = \alpha_V = \alpha$ and $\alpha_{Th} = \alpha_T$:

$$\sigma_h = \frac{\nu}{1-\nu}\left(\sigma_V - \alpha p_p\right) + \alpha p_p + \frac{E}{1-\nu^2}\left(\varepsilon_h + \nu\varepsilon_H\right) + \frac{E\alpha_T}{1-\nu}\Delta T, \quad (3)$$

$$\sigma_H = \frac{\nu}{1-\nu}\left(\sigma_V - \alpha p_p\right) + \alpha p_p + \frac{E}{1-\nu^2}\left(\varepsilon_H + \nu\varepsilon_h\right) + \frac{E\alpha_T}{1-\nu}\Delta T. \quad (4)$$

Eqs. (3) and (4) indicate that the minimum and maximum horizontal stresses are highly dependent on vertical stress, pore pressure, and lithology. These equations indicate that the formation with a smaller Poisson's ratio has smaller minimum and maximum horizontal stresses. A sandstone formation generally has smaller Poisson's ratio than a shale formation; hence, the sandstone has a much smaller minimum horizontal stress than the shale (Figure 4, [12]). If a rock has a higher minimum stress (e.g., a shale), it will have a much higher breakdown pressure (i.e., difficult for hydraulic fractures to be initiated, as illustrated in Eq. (20)). Therefore, the rock that has a higher minimum horizontal stress can act to be a hydraulic fracture barrier to contain the hydraulic fractures within the rock (as shown in stage 2 of Figure 1). In contrast, if the hydraulic fracturing is conducted in a reservoir with a low minimum horizontal stress and no higher minimum horizontal stress formations are located at the top and bottom of the reservoir (i.e., no hydraulic fracture barriers), hydraulic fractures will grow beyond the reservoir zone, causing inefficient stimulation (e.g., stages 3 and 4 of Figure 1).

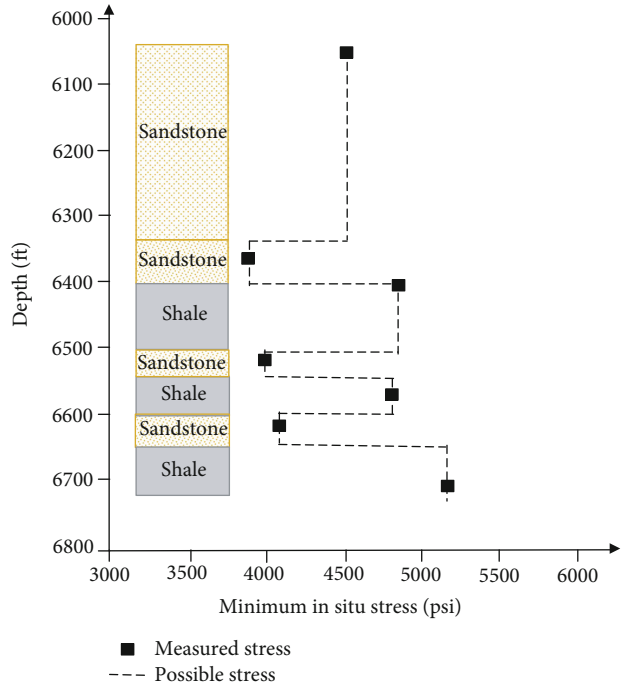

Figure 4: The minimum horizontal stress obtained in overcoring measurements from openhole hydraulic fracture tests in the Canyon Sands of West Texas (modified from [13]). The unit conversions are 1 psi = 0.00689 MPa and 1 ft. = 0.305 m.

In a special condition if $\varepsilon_h = \varepsilon_H = 0$, then Eqs. (3) and (4) become the isotropic uniaxial strain solution:

$$\sigma_h = \frac{\nu}{1-\nu}\left(\sigma_V - \alpha p_p\right) + \alpha p_p + \sigma_T, \tag{5}$$

where the temperature stress is $\sigma_T = [E\alpha_T/(1-\nu)]\Delta T$.

Without considering the temperature effect, Eq. (5) becomes the well-known minimum horizontal stress model in the uniaxial strain condition:

$$\sigma_h = \frac{\nu}{1-\nu}\left(\sigma_V - \alpha p_p\right) + \alpha p_p. \tag{6}$$

This equation is also called the uniaxial strain model. It has been found that the minimum horizontal stress obtained from this model (Eq. (6)) is the minimum value or lower bound minimum horizontal stress [14]. This finding makes the uniaxial strain model more useful and can be used for stress polygon analysis.

2.2. Calculations of the Horizontal Stresses from the Tectonic Horizontal Stresses. The uniaxial strain model in Eq. (6) was popular, but it is oversimplified to calculate the minimum horizontal stress, especially in a tectonic region. Therefore, a more applicable model is needed. If the tectonic stress or excess stress is considered, the minimum horizontal stress equation in the isotropic rock (Eq. (3)) may be rewritten in the following form [15]:

$$\sigma_h = \frac{\nu}{1-\nu}\left(\sigma_V - \alpha p_p\right) + \alpha p_p + \sigma_T + \sigma_{\text{tect}}{}^{\min}, \tag{7}$$

where $\sigma_{\text{tect}}{}^{\min}$ is the excess or tectonic stress in the direction of the minimum horizonal stress and can be obtained from the following equation:

$$\sigma_{\text{tect}}{}^{\min} = \frac{E}{1-\nu^2}(\varepsilon_h + \nu\varepsilon_H). \tag{8}$$

Similarly, the following equation can be used to calculate the maximum horizontal stress, if the tectonic horizontal stress is known:

$$\sigma_H = \frac{\nu}{1-\nu}\left(\sigma_V - \alpha p_p\right) + \alpha p_p + \sigma_T + \sigma_{\text{tect}}{}^{\max}, \tag{9}$$

where $\sigma_{\text{tect}}{}^{\max}$ is the tectonic stress or excess stress in the direction of the maximum horizonal stress, and

$$\sigma_{\text{tect}}{}^{\max} = \frac{E}{1-\nu^2}(\varepsilon_H + \nu\varepsilon_h). \tag{10}$$

It can be seen that if the excess stresses or horizontal strains can be obtained, then the horizontal stresses in the isotropic rock can be calculated from Eqs. (7) and (9). It has been found that if the measured excess stresses are available (e.g., [16]), Eq. (7) could be a good method for calculating the minimum horizontal stress in isotropic rocks, such as intact sandstones. However, horizontal strains ($\varepsilon_h, \varepsilon_H$) are difficult to obtain. Therefore, Eq. (7) may need to simplify, and the minimum horizontal stress can be obtained from the following empirical equation with a calibration factor (k_h):

$$\sigma_h = \frac{\nu}{1-\nu}\left(\sigma_V - \alpha p_p\right) + \alpha p_p + \sigma_T + k_h\sigma_V, \tag{11}$$

where k_h is a calibration factor of the minimum stress. It can be back calculated from measured data in the field tests (such as minifrac test, LOT, XLOT, and DFIT; e.g., $k_h = 0.035$ in a case study from [17]).

A similar empirical equation can be applied to estimate the maximum horizontal stress:

$$\sigma_H = \frac{\nu}{1-\nu}\left(\sigma_V - \alpha p_p\right) + \alpha p_p + \sigma_T + k_H\sigma_V, \tag{12}$$

where k_H is the maximum stress coefficient, another calibration factor, and can be approximately obtained by $k_H = (1/\nu)k_h$ (by comparison Eqs. (8) and (10) with assumption of $\varepsilon_h = 0$).

2.3. Determination of Lower and Upper Bound Horizontal Stresses. Based on Anderson's faulting theory [18], the in situ stress state can be categorized to three stress regimes, i.e.,

(1) Normal faulting stress regime: this is a case that vertical stress is the driving stress to form a normal fault. In this case, when the minimum stress reaches a critically low value, shear failure or fault slip happens. In

this stress regime, the vertical stress is the largest principal stress, and three principal stresses have the following relation: $\sigma_V \geq \sigma_H \geq \sigma_h$

(2) Strike-slip faulting stress regime: in this stress regime, the vertical stress is the intermediate principal stress, but the maximum horizontal stress is the major principal stress to form a strike-slip fault. In this case, the three stresses follow this relation: $\sigma_H \geq \sigma_V \geq \sigma_h$

(3) Thrust or reverse faulting stress regime: this is a case that vertical stress is the least principal stress. This is the highest in situ stress regime, and the three stresses have the following relation: $\sigma_H \geq \sigma_h \geq \sigma_V$

(4) Assuming that the critically oriented faults constrain the three principal stresses of σ_h, σ_H, and σ_V, the Mohr-Coulomb failure criterion for the faults can be used to constrain the in situ stress relation. The following horizontal stress bounds can be obtained from the Mohr-Coulomb failure criterion (e.g., [19, 20]). Therefore, the lower bound minimum horizontal stress (σ_h^{LB}) can be obtained as the following equation:

$$\sigma_h^{LB} = \left(\sqrt{\mu_f^2 + 1} + \mu_f\right)^{-2} \left(\sigma_V - p_p\right) + p_p, \tag{13}$$

where μ_f is the coefficient of friction of the fault; $\mu_f = \tan \varphi_f$; φ_f is the angle of internal friction of the fault.

The upper bound maximum horizontal stress (σ_H^{UB}) is written in a similar equation:

$$\sigma_H^{UB} = \left(\sqrt{\mu_f^2 + 1} + \mu_f\right)^{2} \left(\sigma_V - p_p\right) + p_p. \tag{14}$$

It is difficult to accurately obtain the coefficient of friction of the fault (μ_f); therefore, Zhang and Zhang [14] proposed to use Poisson's ratio of the rock to determine the lower bound minimum horizontal stress and the upper bound maximum horizontal stress in the following equations:

$$\sigma_h^{LB} = \frac{\nu}{1-\nu}\left(\sigma_V - p_p\right) + p_p, \tag{15}$$

$$\sigma_H^{UB} = \frac{1-\nu}{\nu}\left(\sigma_V - p_p\right) + p_p, \tag{16}$$

where Poisson's ratio (ν) may be calculated from the sonic log, i.e., $\nu = [(V_p/V_s)^2/2 - 1]/[(V_p/V_s)^2 - 1]$, and V_p and V_s are the compressive and shear velocities, respectively.

The new stress polygon, which is dependent highly on Poisson's ratio, can be calculated from Eqs. (15) and (16) and plotted [11]. Figure 5 presents an example of the new stress polygon. In this plot, two stress polygons are plotted. It shows different Poisson's ratio effects on the areas of the stress polygons. The rock with smaller Poisson's ratio (PR = 0.3) has a large stress polygon, and the rock with larger Poisson's ratio (PR = 0.4) has a smaller stress polygon. This figure demonstrates that if Poisson's ratio can be accurately obtained, the stress polygon can be plotted accurately. The new stress polygon method can decrease uncertainty in construction of the stress polygon because the uncertainty of Poisson's ratio is smaller than that of the coefficient of friction of the fault, which is used to plot conventional stress polygon. Combined to borehole breakouts and drilling-induced tensile fractures, this Poisson's ratio-dependent stress polygon can be used to estimate in situ stresses.

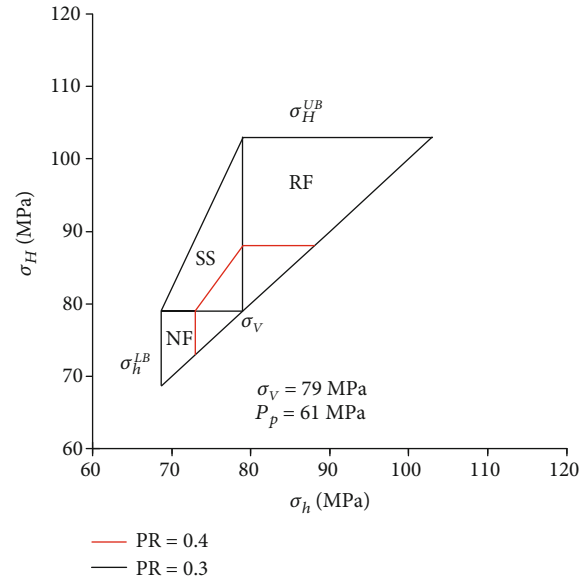

Figure 5: Upper bound and lower bound principal stresses and stress polygons calculated from Eqs. (15) and (16) in two different Poisson's ratios (PR in the figure). In the figure, RF, SS, and NF represent the reverse, strike-slip, and normal faulting stress regimes, respectively.

3. Determinations of Horizontal Stresses from Leak-Off Tests

3.1. Minimum Horizontal Stress in the Normal or Strike-Slip Faulting Stress Regime. In the normal or strike-slip faulting stress regime, the minimum stress is the minimum horizontal principal stress. Direct borehole hydraulic injection tests can be used to determine the minimum horizontal stress. The tests include microhydraulic fracturing (e.g., [21]), mini-frac, leak-off test (LOT), extended leak-off test (XLOT), or diagnostic fracture injection test (DFIT). In the borehole hydraulic injection test, the minimum horizontal stress is assumed to be the fracture closure pressure. The closure pressure can be determined on the decline curve in a hydraulic injection test after the fluid injection is shut-in [22].

In a typical LOT, the borehole injection pressure increases linearly if the tested borehole has no leaks, and the test formation is not very permeable. At a certain time of injection, the pressure in the borehole departs from the linearity (Figure 6), and the pressure at this departure point is the fracture initiation pressure (p_i). As the injection pressure continues to increase to the maximum pressure, hydraulic fractures are created or the formation is broken down. This

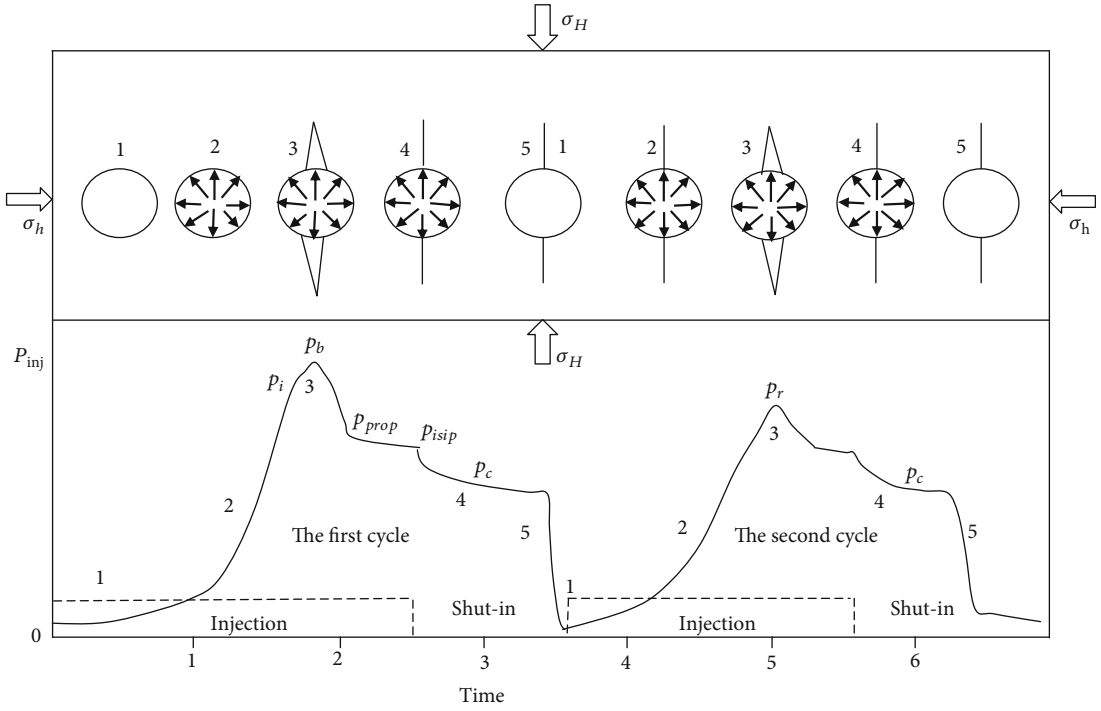

Figure 6: Schematic plot of a typical XLOT of two injection cycles. Upper figure: schematic borehole tensile failure stages (fracture growth and closure) versus the injection pressure; lower figure: the relationship of pumping pressure, fracture initiation pressure, formation breakdown pressure, and testing time.

maximum injection pressure is the formation breakdown pressure (p_b) [23, 24]. After the formation is broken down, the fracture is propagating, and a fairly constant pressure (p_{prop}) remains in the borehole at the same flow rate for a certain time. After the pump is shut in and injection is stopped, the pressure drops to the instantaneous shut-in pressure (p_{isip}). Then, the pressure in the borehole begins to decrease because the fracture is gradually closing. When the fracture is closed, the pressure acting to the fracture is the closure pressure, which is equal to the minimum horizontal stress, i.e.,

$$\sigma_h = p_c, \tag{17}$$

where p_c is the closure pressure.

A second injection cycle may be required in the XLOT (Figure 6) in order to obtain a repeatable closure pressure and rock tensile strength. Because fractures have been created by the first test cycle, it is commonly assumed that tensile strength is zero in the second test or the fracture reopening stage; therefore,

$$T_0 = p_b - p_r, \tag{18}$$

where T_0 is the tensile strength of the tested formation; p_r is the fracture reopening pressure (refer to Figure 6); p_b is the formation breakdown pressure.

3.2. Minimum Stress in the Reverse Faulting Stress Regime. Different from one in the normal or strike-slip faulting stress regime, the LOT performed in a reverse faulting stress regime has a different result in the minimum stress. Because the minimum stress is the vertical stress in a reverse faulting stress regime, the fractures generated by injection should be horizontal fractures. Therefore, in this case, the closure pressure is equal to the vertical stress, i.e.,

$$\sigma_V = p_c. \tag{19}$$

It can be concluded that the closure pressure observed from a borehole hydraulic fracturing test in a reverse faulting stress regime is not the minimum horizontal stress. Therefore, alternative stress measurement methods are required to obtain the minimum horizontal stress, such as borehole overcoring measurement (e.g., [25]) and anelastic strain recovery (ASR) method.

3.3. Maximum Horizontal Stress Estimates from XLOT Measurements

3.3.1. For the Hydraulic Fracture in the Impermeable Rock. From the multicycle XLOT or DFIT in the normal or strike-slip faulting stress regime, both the minimum and maximum horizontal stresses can be obtained. The early work was done by Haimson and Fairhurst [26] to determine the fracture initiation pressure from the minifrac test in a vertical well. They assumed that the rock is elastic and isotropic media and derived an equation similar to Eq. (20), but the thermal stress σ_T was not considered. This equation can be used to calculate the fracture initiation pressure with no fluid penetration in the formation. They considered that this

equation might be used to estimate formation breakdown pressure:

$$p_i = 3\sigma_h - \sigma_H - p_p + \sigma_T + T_0. \quad (20)$$

However, laboratory hydraulic fracturing experiments have showed that the breakdown pressure calculated from Eq. (20) is underestimated (e.g., [27]). A new model (Eq. (21)) for calculating formation breakdown pressure was presented (Zhang et al. [28]). Compared to Eq. (20), the new model predicts a higher breakdown pressure, which has a better fit to the experimental result.

$$p_b = 3\sigma_h - \sigma_H - p_p + \sigma_T + kT_0, \quad (21)$$

where k is the rock strength factor, and Eq. (21) is simplified to Eq. (20) if $k = 1$. Our recent laboratory hydraulic fracturing tests in large samples of tight sandstones show that the rock strength factor can be as high as $k = 2.85$ [29].

Eq. (21) predicts a higher breakdown pressure than that in Eq. (20) because the tensile strength has a stronger effect in Eq. (21). Hence, the result calculated from Eq. (21) can be considered to be the upper bound breakdown pressure. Rearranging Eq. (21), the maximum horizontal stress can be given when the XLOT measurements are available using the following equation:

$$\sigma_H = 3\sigma_h - p_b - p_p + \sigma_T + kT_0. \quad (22)$$

3.3.2. For the Hydraulic Fracture in the Porous Rock. The derivation of Eqs. (20) and (22) assumes that before the fracture opens, fluid pressure in the borehole does not penetrate into the hydraulic fracture. If the fracture is slightly conductive, the pressure penetration of the fracture will transmit to the fracture surface because the net area of contact of the two surfaces is usually a small fraction of their nominal area [30]. Therefore, the pressure in the fracture at the borehole wall (p_w) is the same to pore pressure, i.e., $p_p = p_w = p_r$. Substituting Eq. (18) and $p_p = p_r$ into Eq. (22), the maximum horizontal stress may be derived in the following form:

$$\sigma_H = 3\sigma_h + (k-1)p_b - (k+1)\mathrm{p}_r + \sigma_T. \quad (23)$$

For the case of $k = 1$, Eq. (23) has a simple form:

$$\sigma_H = 3\sigma_h - 2p_r + \sigma_T. \quad (24)$$

If the hydraulic fracture is more conductive, the fluid pressure may fully penetrate into the fracture tip. In this case, the fracture reopening is primarily controlled by total force created by the fluid pressure on the fracture surfaces [31]. Therefore, the reopening pressure is the same to the closure pressure or the minimum horizontal stress:

$$\sigma_h = p_r. \quad (25)$$

If fluid flow from the hydraulic fracture into the formation is considered, the following poroelastic solution was derived for calculating formation breakdown pressure (Eq. (26)) with consideration of the effect of the porous rocks in the case of penetrating fluid [26, 32]. The breakdown pressure obtained from this equation can be treated to be the lower case of the breakdown pressure, i.e.,

$$p_b = \frac{3\sigma_h - \sigma_H - 2\eta p_p + T_0}{2(1-\eta)}, \quad (26)$$

where $\eta = (1-2\nu)/[2(1-\nu)]$. Because $0 \le \nu \le 0.5$, $1 \le 2(1-\eta) \le 2$, the breakdown pressure calculated from Eq. (26) is less than the one obtained from Eq. (20).

If the thermal stress is considered, the maximum horizontal stress in the permeable rock can be derived from Eq. (26):

$$\sigma_H = 3\sigma_h - 2(1-\eta)p_b - 2\eta p_p + T_0 + \sigma_T. \quad (27)$$

From the above analysis, Eqs. (27) and (24) can be considered to be the lower side maximum horizontal stress, and Eq. (22) can be treated to be the upper side maximum horizontal stress.

4. Methods for Determining the Maximum Horizontal Stress

Compared to the minimum horizontal stress, the maximum horizontal stress has more challenges to be accurately determined, particularly in naturally fractured rocks and in the reverse faulting stress regime. In this situation, different methods are needed to verify and calibrate each method and eventually to obtain an integrated approach. In the following section, several methods are provided to determine the maximum horizontal stress.

4.1. Maximum Horizontal Stress Estimation from Borehole Breakouts. If the near-wellbore stress caused by drilling exceeds the compressive strength of the wellbore rock because the applied mud weight is lower than the required, wellbore breakouts (shear failures) occur around the wellbore (e.g., [3, 33]). However, if the applied mud weight is too high, the near-wellbore stress may exceed rock tensile failure criterion, and tensile fractures caused by drilling will develop in the wellbore. Figure 7 shows drilling-induced tensile fractures and wellbore breakouts in a vertical wellbore. It can be seen that drilling-induced tensile fractures align in the maximum horizontal stress direction; however, the wellbore breakout is parallel to the minimum horizontal stress direction. Based on this principle, if the orientations of the drilling-induced tensile fractures, and wellbore breakouts are known; then, the directions of the maximum and minimum horizontal stresses can be inferred. The directions can also be obtained from the laboratory approach combining paleomagnetic and acoustic anisotropy tests (e.g., [34]).

Assuming that when wellbore breakout occurs, the stresses around the wellbore wall in a vertical well follows the Mohr-Coulomb failure criterion, the following equation can be derived to estimate the maximum horizontal stress

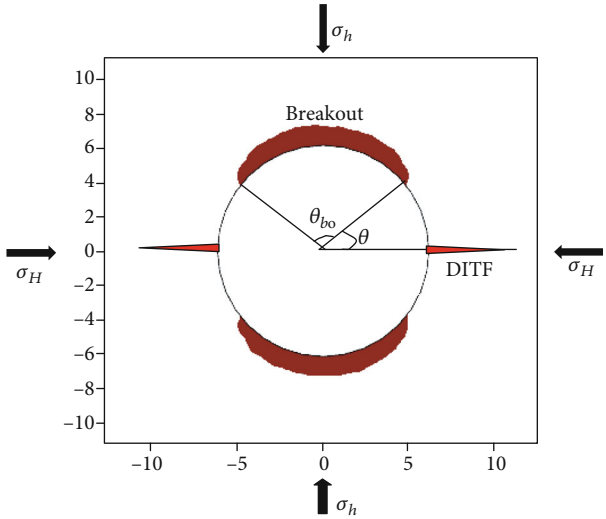

Figure 7: Schematic figure showing wellbore tensile failure (drilling-induced tensile fractures, DITF in the figure) and shear failure (wellbore breakouts) in a vertical borehole cross section.

(refer to Zhang [11] for derivations). The following equation can be used to calculate the maximum horizontal stress when the width of wellbore breakout in a vertical borehole is available:

$$\sigma_H = \frac{UCS + (q+1)p_m - (q-1)p_p - (1 - 2\cos\theta_{bo})\sigma_h + \sigma_T}{1 + 2\cos\theta_{bo}}, \tag{28}$$

where UCS is the uniaxial compressive strength; p_m is the downhole mud pressure in the borehole; θ_{bo} is the borehole breakout angle, $\theta_{bo} = 180^\circ - 2\theta$, and θ is the angle as shown in Figure 7; $q = (1 + \sin\varphi)/(1 - \sin\varphi)$ and φ is the angle of internal friction.

Eq. (28) becomes a simplified equation proposed by Barton et al. [35] for a case if the borehole is in uniaxial loading condition (i.e., $q = 0$). Horizontal stresses determination from wellbore breakouts in inclined boreholes is more complicated and can be found in Zajac and Stock [36]. Wellbore breakout widths or breakout angles can be interpreted from caliper log or image log, and the downhole mud pressure can be obtained from the ECD (equivalent circulating density) by the MWD or mud log. The pore pressure can be measured from well logging pressure measurement or estimated from well log data [5].

4.2. Maximum Horizontal Stress Estimation from Drilling-Induced Fractures. The drilling-induced tensile fractures will generate if the mud weight used for borehole drilling is too high (Figure 7). Generally, drilling-induced tensile fractures are thin and long fractures and can cause incidents of mud losses or lost circulation while drilling [37, 38]. Drilling-induced tensile fractures will start to generate if the mud pressure equals the formation initiation pressure. In this case, we can use Eq. (20) to estimate the maximum horizontal stress for the drilling-induced tensile fractures in a vertical well in the normal or strike-slip faulting stress regime. Replacing p_i with p_m in Eq. (20), the following equation can be obtained:

$$\sigma_H = 3\sigma_h - p_m - p_p + \sigma_T + T_0, \tag{29}$$

where p_m is the downhole mud pressure.

Plotting drilling-induced tensile fractures (Eq. (29)) and borehole breakouts (Eq. (28)) into the principal stress polygon plot and the maximum horizontal stress can be estimated.

4.3. Maximum Horizontal Stress from Wellbore Breakouts and Drilling-Induced Tensile Fractures. When two different borehole failures (borehole breakouts and drilling-induced tensile fractures) happen simultaneously, Poisson's ratio-dependent stress polygon given in Section 2.3 combined to these borehole failure equations (Eqs. (28) and (29)) can be used to estimate the maximum and minimum horizontal stresses. Using the methods presented in Sections 4.1 and 4.2, a new stress polygon can be used to calculate horizontal stresses. A case study is examined to illustrate this method. The studied field is a gas reservoir located in the Sichuan basin [39]. Wellbore breakouts and drilling-induced tensile fractures occurred simultaneously in certain depths in some boreholes, and Figure 8 presents one of the examples. The parameters in this borehole are as follows: depth $D = 3219$ m, vertical stress $\sigma_V = 79$ MPa, downhole mud pressure $p_m = 66$ MPa, pore pressure $p_p = 61$ MPa, and Poisson's ratio $\nu = 0.2$.

In order to estimate horizontal stresses, a stress polygon needs firstly to be plotted. The lower and upper bound horizontal stresses from Eqs. (15) and (16) can be used to determine two important lines, as shown in Figure 9. Based on wellbore shear and tensile data, wellbore breakout lines and DITF lines can be added to the stress polygon plot. In Figure 9, the breakout lines are drawn based on Eq. (28), in which breakouts happen at the applied mud weight of $p_m = 66$ MPa for the rock compressive strength of UCS from 60 to 90 MPa. The DITF lines can be plotted using Eq. (29) with tensile strength T_0 from 2 to 8 MPa, as shown in Figure 9. The area surrounded by the two breakout lines and the two DITF lines is the ranges of the minimum and maximum horizontal stresses. Figure 9 indicates that the minimum and maximum horizontal stresses are constrained to a small area. If rock strength uncertainties are small, the horizontal stresses then can be better constraint. If the minimum horizontal stress is known, the stress polygon can be applied to estimate the maximum horizontal stress. The minimum horizontal stress from the LOT measurement in the interested depth in this borehole was available, i.e., $\sigma_h = 73$ MPa, and then the maximum horizontal stress can be estimated from Figure 9 as $\sigma_H = 93.9 - 99.9$ MPa. It can also be found in Figure 9 that the in situ stresses (the area surrounded by the DITF lines and wellbore breakout lines) are in the strike-slip faulting stress regime; therefore, this method may also be used to determine the stress regime.

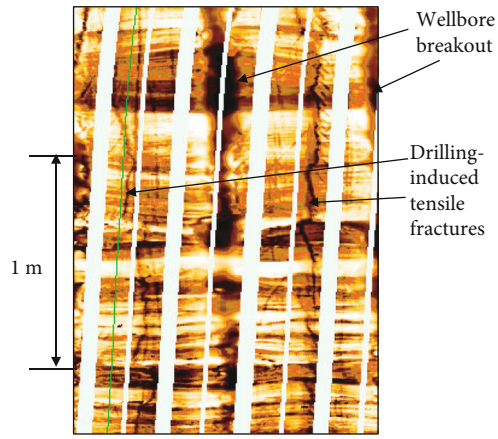

Figure 8: Wellbore breakouts and drilling-induced tensile fractures occurred simultaneously in a vertical borehole.

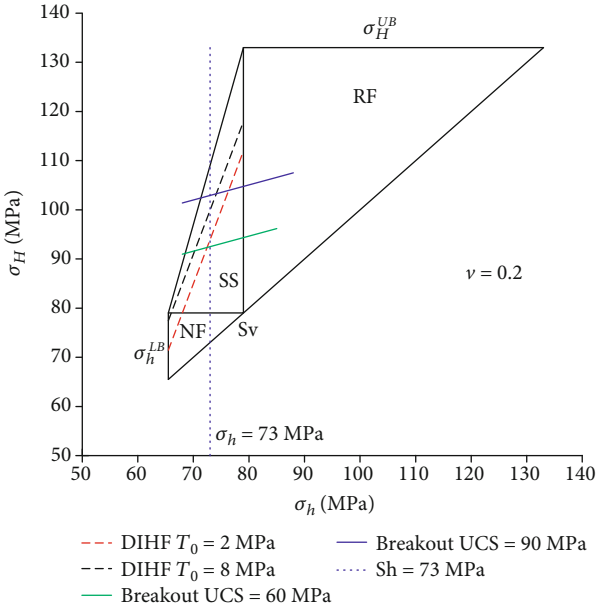

Figure 9: Constrained ranges of the minimum and maximum horizontal stresses obtained from Poisson's ratio-based new stress polygon plot combined drilling-induced tensile fractures and wellbore breakouts in the vertical well shown in Figure 8.

4.4. Maximum Horizontal Stress from Elasticity Theory. If the stresses and strains are in equilibrium in an elastic formation, the vertical stress and two horizontal stresses follow the generalized Hooke's law. Therefore, the horizontal strain and the maximum effective horizontal stress have the following relation:

$$\varepsilon_H = \frac{1}{E}\left[\sigma'_H - \nu\left(\sigma'_h + \sigma'_V\right)\right], \tag{30}$$

where σ'_V, σ'_H, and σ'_h are the vertical effective stress and minimum and maximum effective horizontal stresses, respectively.

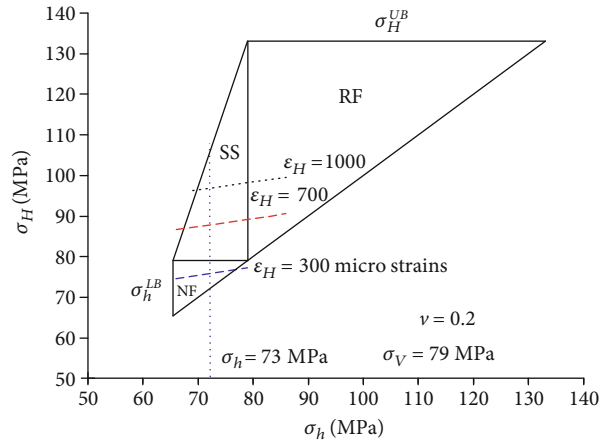

Figure 10: Stress polygon diagram for estimating the maximum horizontal stress using Eq. (31) for three maximum horizontal strains (dash lines).

The in situ stress relation can be derived from Eq. (30) if each effective stress is replaced by its corresponding total stress:

$$\sigma_H = \nu\left(\sigma_V + \sigma_h - 2\alpha p_p\right) + \alpha p_p + E\varepsilon_H. \tag{31}$$

Eq. (31) demonstrates that the maximum horizontal stress can be obtained if the maximum horizontal strain, the minimum horizontal stress, and the vertical stress are known. The subsurface rocks have experienced many different deformations (including elastic and plastic deformations) in the geological history; hence, there are uncertainties in Eq. (31). However, Eq. (31) can be used either as one of the methods for calculating the maximum horizontal stress or for verifying other methods.

The maximum strain can be obtained from GPS measurements (e.g., [40]) or from back-calculation of the measured data of in situ stresses [16]; then, the maximum horizontal stress can be calculated from Eq. (31). This equation can also be drawn on the stress polygon plot to constrain in situ stress estimate as a supplementary method of the previous section. Using the same case application and the same stress polygon of Figure 9, the maximum horizontal stress and strain relation of Eq. (31) can be plotted on the stress polygon, as shown in Figure 10. The same parameters as those used in Figure 9 are applied in the stress polygon of Figure 10, i.e., $\sigma_V = 79$ MPa, $p_p = 61$ MPa, $\nu = 0.2$, $E = 30$ GPa, and $\alpha = 1$. The in situ stress relations calculated from Eq. (31) are drawn in the stress polygon diagram in Figure 10. The figure shows three dashed lines for three different maximum horizontal strain cases ($\varepsilon_H = 300$, $\varepsilon_H = 700$, and $\varepsilon_H = 1000$ microstrains). Figure 10 demonstrates that as the maximum horizontal strain increases, the stress regime varies from the normal faulting stress regime to the strike-slip and the reverse faulting stress regimes. By integrating this method to drilling-induced tensile fractures and wellbore breakouts shown in Figure 9, the maximum horizontal stress

can be obtained. If $\sigma_h = 73$ MPa and $\varepsilon_H = 1000$ microstrains, then the maximum horizontal stress from Figure 10 is $\sigma_H = 98.2$ MPa.

5. Conclusions

Methods for theoretically determining the in situ stresses are overviewed. Field measurements of the minimum and maximum horizontal stresses, particularly borehole injection tests are described, and their suitability of applications and uncertainties are analyzed. The XLOT measurement is a reliable method for determining horizontal stresses in the normal or strike-slip faulting stress regime. Some theoretical methods to estimate the minimum and maximum horizontal stresses are proposed. Combined the proposed methods to the new stress polygon, the horizontal stresses can be obtained. The proposed approach that combines theoretical methods and field measurements provides an integrated approach to estimate the minimum and maximum horizontal stresses.

Data Availability

Access to data is restricted.

Conflicts of Interest

The author(s) declare(s) that they have no conflicts of interest.

Acknowledgments

This paper was partially supported by the National Science Foundation of China (51774136, 51974126), the Program for Innovative Research Team in University sponsored by Ministry of Education of China (IRT-17R37), and Hebei Province Natural Science Foundation Major Project (D2017508099).

References

[1] M. K. Hubbert and D. G. Willis, "Mechanics of hydraulic fracturing," *Transactions of the AIME*, vol. 210, no. 1, pp. 153–168, 1957.

[2] C. Zinn, D. R. Blood, and P. Morath, "Evaluating the impact of wellbore azimuth in the Marcellus Shale," in *Paper presented at the SPE Eastern Regional Meeting*, Columbus, Ohio, USA, 2011.

[3] X. Li, H. Jaffal, Y. Feng, C. el Mohtar, and K. Gray, "Wellbore breakouts: Mohr-Coulomb plastic rock deformation, fluid seepage, and time-dependent mudcake buildup," *Journal of Natural Gas Science and Engineering*, vol. 52, pp. 515–528, 2018.

[4] S. Stolyarov, E. Cazeneuve, K. Sabaa, D. Katz, and J. Yang, "A novel technology for hydraulic fracture diagnostics in the vicinity and beyond the wellbore," in *Paper presented at the SPE Hydraulic Fracturing Technology Conference and Exhibition*, The Woodlands, Texas, USA, 2019.

[5] J. Zhang, "Pore pressure prediction from well logs: Methods, modifications, and new approaches," *Earth-Science Reviews*, vol. 108, no. 1-2, pp. 50–63, 2011.

[6] D. W. Lv, Z. X. Li, D. D. Wang et al., "Sedimentary model of coal and shale in the Paleogene Lijiaya formation of the Huangxian Basin: insight from petrological and geochemical characteristics of coal and shale," *Energy & Fuels*, vol. 33, no. 11, pp. 10442–10456, 2019.

[7] D. W. Lv, D. D. Wang, Z. X. Li, H. Y. Liu, and Y. Li, "Depositional environment, sequence stratigraphy and sedimentary mineralization mechanism in the coal bed- and oil shale-bearing succession: a case from the Paleogene Huangxian Basin of China," *Journal of Petroleum Science and Engineering*, vol. 148, pp. 32–51, 2017.

[8] H. Zhu, X. Tang, Q. Liu et al., "4D multi-physical stress modelling during shale gas production: a case study of Sichuan Basin shale gas reservoir, China," *Journal of Petroleum Science and Engineering*, vol. 167, pp. 929–943, 2018.

[9] E. A. Ejofodomi, M. Yates, R. Downie, T. Itibrout, and O. A. Catoi, "Improving well completion via real-time microseismic monitoring: a West Texas case study," in *Paper presented at the Tight Gas Completions Conference*, San Antonio, TX, 2010.

[10] N. R. Warpinski, R. A. Schmidt, and D. A. Northrop, "In-situ stresses: the predominant influence on hydraulic fracture containment," *Journal of Petroleum Technology*, vol. 34, no. 3, pp. 653–664, 1982.

[11] J. Zhang, *Applied Petroleum Geomechanics*, The Gulf Professional Publishing of Elsevier, 2019.

[12] T. L. Blanton and J. E. Olson, "Stress Magnitudes from logs: effects of tectonic strains and temperature," *SPE Reservoir Evaluation & Engineering*, vol. 2, no. 1, pp. 62–68, 1999.

[13] W. K. Miller II, R. E. Peterson, J. E. Stevens, C. B. Lackey, and C. W. Harrison, "In-situ stress profiling and prediction of hydraulic fracture azimuth for the West Texas Canyon Sands formation," *SPE Production & Facilities*, vol. 9, no. 3, pp. 204–210, 1994.

[14] Y. Zhang and J. Zhang, "Lithology-dependent minimum horizontal stress and in-situ stress estimate," *Tectonophysics*, vol. 703-704, pp. 1–8, 2017.

[15] S. R. Daines, "Prediction of fracture pressures for wildcat wells," *Journal of Petroleum Technology*, vol. 34, no. 4, pp. 863–872, 1982.

[16] D. R. Dolinar, "Variation of horizontal stresses and strains in mines in bedded deposits in the eastern and midwestern United States," in *Proceedings of the 22nd International Conference on Ground Control in Mining*, Morgantown, WV, 2003.

[17] Z. Meng, J. Zhang, and R. Wang, "In-situ stress, pore pressure and stress-dependent permeability in the Southern Qinshui Basin," *International Journal of Rock Mechanics and Mining Sciences*, vol. 48, no. 1, pp. 122–131, 2011.

[18] E. M. Anderson, *The Dynamics of Faulting and Dyke Formation with Application to Britain*, Oliver and Boyd, Edinburgh, 2nd edition edition, 1951.

[19] R. H. Sibson, "Frictional constraints on thrust, wrench and normal faults," *Nature*, vol. 249, no. 5457, pp. 542–544, 1974.

[20] M. D. Zoback, C. A. Barton, M. Brudy et al., "Determination of stress orientation and magnitude in deep wells," *International Journal of Rock Mechanics and Mining Sciences*, vol. 40, no. 7-8, pp. 1049–1076, 2003.

[21] B. C. Haimson and F. H. Cornet, "ISRM suggested methods for rock stress estimation–part 3: hydraulic fracturing (HF) and/or hydraulic testing of pre-existing fractures (HTPF)," *International Journal of Rock Mechanics and Mining Sciences*, vol. 40, no. 7-8, pp. 1011–1020, 2003.

[22] W. S. Whitehead, E. R. Hunt, R. J. Finley, and S. A. Holditch, "In-situ stresses: a comparison between log-derived values and actual field-measured values in the Travis peak formation of East Texas," in *Paper presented at the SPE Unconventional Gas Technology Symposium*, Louisville, Kentucky, 1986.

[23] S. Yin, J. Zhang, and D. Liu, "A study of mine water inrushes by measurements of in situ stress and rock failures," *Natural Hazards*, vol. 79, no. 3, pp. 1961–1979, 2015.

[24] J. Zhang and J.-C. Roegiers, "Discussion on "Integrating borehole-breakout dimensions, strength criteria, and leak-off test results, to constrain the state of stress across the Chelungpu Fault, Taiwan"," *Tectonophysics*, vol. 492, no. 1-4, pp. 295–298, 2010.

[25] C. Ljunggren, Y. Chang, T. Janson, and R. Christiansson, "An overview of rock stress measurement methods," *International Journal of Rock Mechanics and Mining Sciences*, vol. 40, no. 7-8, pp. 975–989, 2003.

[26] B. C. Haimson and C. Fairhurst, "Initiation and extension of hydraulic fractures in rocks," *Society of Petroleum Engineers Journal*, vol. 7, no. 3, pp. 310–318, 1967.

[27] M. D. Zoback, F. Rummel, R. Jung, and C. B. Raleigh, "Laboratory hydraulic fracturing experiments in intact and pre-fractured rock," *International Journal of Rock Mechanics and Mining Sciences & Geomechanics Abstracts*, vol. 14, no. 2, pp. 49–58, 1977.

[28] Y. Zhang, J. Zhang, B. Yuan, and S. Yin, "In-situ stresses controlling hydraulic fracture propagation and fracture breakdown pressure," *Journal of Petroleum Science and Engineering*, vol. 164, pp. 164–173, 2018.

[29] H. Kang, J. Zhang, X. Fan, and Z. Huang, "Cyclic injection to enhance hydraulic fracturing efficiency: insights from laboratory experiments," *Geofluids*, vol. 2020, Article ID 8844293, 10 pages, 2020.

[30] T. Ito, K. Evans, K. Kawai, and K. Hayashi, "Hydraulic fracture reopening pressure and the estimation of maximum horizontal stress," *International Journal of Rock Mechanics and Mining Sciences*, vol. 36, no. 6, pp. 811–826, 1999.

[31] J. Rutqvist, C. F. Tsang, and O. Stephansson, "Uncertainty in the maximum principal stress estimated from hydraulic fracturing measurements due to the presence of the induced fracture," *International Journal of Rock Mechanics and Mining Sciences*, vol. 37, no. 1-2, pp. 107–120, 2000.

[32] E. Detournay and A. H. D. Cheng, "Poroelastic response of a borehole in a non-hydrostatic stress field," *International Journal of Rock Mechanics and Mining Sciences & Geomechanics Abstracts*, vol. 25, no. 3, pp. 171–182, 1988.

[33] J. Zhang, "Borehole stability analysis accounting for anisotropies in drilling to weak bedding planes," *International Journal of Rock Mechanics and Mining Sciences*, vol. 60, pp. 160–170, 2013.

[34] Y. Han, Y. Feng, X. Li, and S. Zhang, "Evaluation of in-situ stress orientation: a laboratory approach combining paleomagnetic test and acoustic anisotropy test," *Journal of Petroleum Science and Engineering*, vol. 195, article 107870, 2020.

[35] C. A. Barton, M. D. Zoback, and K. L. Burns, "In-situ stress orientation and magnitude at the Fenton Geothermal Site, New Mexico, determined from wellbore breakouts," *Geophysical Research Letters*, vol. 15, no. 5, pp. 467–470, 1988.

[36] B. J. Zajac and J. M. Stock, "Using borehole breakouts to constrain the complete stress tensor: results from the Sijan Deep Drilling Project and offshore Santa Maria Basin, California," *Journal of Geophysical Research*, vol. 102, no. B5, pp. 10083–10100, 1997.

[37] S. Li and C. Purdy, "Maximum horizontal stress and wellbore stability while drilling: modeling and case study," in *Paper presented at the SPE Latin American and Caribbean Petroleum Engineering Conference*, Lima, Peru, 2010.

[38] J. Zhang and S. Yin, "Fracture gradient prediction: an overview and an improved method," *Petroleum Science*, vol. 14, no. 4, pp. 720–730, 2017.

[39] J. Zhang, H. Zheng, G. Wang et al., "In-situ stresses, abnormal pore pressures and their impacts on the Triassic Xujiahe reservoirs in tectonically active western Sichuan basin," *Marine and Petroleum Geology*, vol. 122, article 104708, 2020.

[40] Y. Pan and W.-B. Shen, "Contemporary crustal movement of southeastern Tibet: constraints from dense GPS measurements," *Scientific Reports*, vol. 7, no. 1, article 45348, 2017.